

## Surface Patterns of Laterally Extended Thin Liquid Films in Three Dimensions

Michael Bestehorn\* and Kai Neuffer

*Lehrstuhl für Theoretische Physik II, Brandenburgische Technische Universität Cottbus, Erich-Weinert-Straße 1, 03046 Cottbus, Germany*

(Received 26 January 2001; published 10 July 2001)

We examine the fully nonlinear behavior of a thin liquid film in three spatial dimension for a large lateral extension. A partial differential equation is used for the spatiotemporal evolution of the height of the film. To take intermolecular forces in the liquid into account, we concentrate on a recently formulated model of Pismen and Pomeau, who derived an expression for the disjoining pressure only from the wetting properties of the fluid. Finally, the motion of a falling film on an inclined plane is studied within this model.

DOI: 10.1103/PhysRevLett.87.046101

PACS numbers: 68.15.+e, 64.70.-p, 68.55.-a

The spatiotemporal behavior of thin liquid films on a solid support and with free surface has widespread technological applications like coating or wetting processes. If the surface of the flat film is unstable to spatial disturbances, pattern formation sets in and drops, holes and eventually film rupture may occur. The spontaneous formation of surface patterns on thin liquid films is known as “spinodal dewetting.” The description used here goes back to the work of Vrij [1] and is based on a free (interface) energy which includes surface tension phenomenologically. In contrast to the stabilizing effect of the surface tension, destabilizing mechanisms may originate from intermolecular forces in the film which give rise to an additional pressure term in the Navier-Stokes equations, the disjoining pressure [2]. Using the diffusive interface description [3], Pismen and Pomeau [4] recently derived an expression for the disjoining pressure with only one free parameter determined by the wetting properties of the fluid. They considered a three phase contact line (solid-liquid-gas) and computed the interaction force between the liquid-gas interface and the solid support. It turns out that this force can be repelling (medium and very short distances) or attracting (short and long distances), allowing for two homogeneous and stationary solutions for the film thickness. The same functional dependence of the disjoining pressure on the film height was examined in the work of Sharma *et al.* and referred to as type IV systems [5–8], derived there from Van der Waals forces in the liquid. In their 3D-numerical investigations, Sharma *et al.* found similar results to our noninclined case; in particular, they obtained drops, holes, and labyrinths, depending on the parameters of the interaction force. The similarity to our findings supports their conjecture that the functional dependence of the disjoining pressure on the film height is crucial for pattern evolution and morphology. In contrast to previous work we shall use the disjoining pressure of Pismen and Pomeau and show numerically that for certain parameter ranges where the flat film is unstable, holes and drops are formed in large lateral geometries. Finally, we present numerical solutions for inclined films, where falling drops

or fronts can be studied, in agreement with recent experiments [9].

*Thin film equation.*—As already mentioned in [7], three dimensional examination of the basic equations seems necessary since in two dimensions the behavior is qualitatively different; e.g., it is hard to determine between holes and drops and the formation of circular structures cannot be demonstrated. We consider pattern formation in thin films obeying the lubrication approximation [2]. Then the height  $h$  of the film can be expressed as a unique function of the horizontal coordinates  $\mathbf{x} = (x, y)$  and time. For the evolution of  $h$  a  $(2 + 1)$  dimensional conservation equation of the form

$$\partial_t h(\mathbf{x}, t) = -\nabla \mathbf{S}(h) \quad (1)$$

applies, where the current density  $\mathbf{S}(h)$  can be expressed by

$$\mathbf{S}(h) = -Q(h)\nabla\phi(h) \quad (2)$$

with the generalized force  $\nabla\phi(h)$  and the mobility  $Q(h)$ . Here  $\nabla$  denotes the horizontal gradient  $(\partial_x, \partial_y)$ . The force is given by the gradient of the chemical potential  $\phi$  which itself may be derived from a free energy  $F$  by  $\phi(h) = \delta F/\delta h$ . If one wishes to include the surface tension  $\sigma$  at the film surface, the Ginzburg-Landau free energy functional

$$F[h] = \int d^2\mathbf{x} \left\{ \frac{1}{2} \sigma (\nabla h)^2 + f(h) \right\} \quad (3)$$

can be used. The notion “disjoining pressure” is commonly used for the negative derivative  $\Pi = -df/dh$ . Because of  $d_t F[h] \leq 0$ , asymptotically time stable spatial patterns can be found by  $\delta F[h] = 0$  with the constraint  $\int d^2\mathbf{x} h = \text{const}$ , which means that the volume has to be conserved. (This is, of course, true only for periodic or Neumann lateral boundary conditions for  $\mathbf{S}$ . Here we assume periodic ones.) Inserting (3) into (2) and (2) into (1) we may write (1) in a more convenient form, where the possible occurrence of spatially inhomogeneous instabilities can be seen immediately. It reads

$$\begin{aligned} \partial_t h = & D(h)\Delta h - Q(h)\Delta^2 h + [d_h D(h)](\nabla h)^2 \\ & - [d_h Q(h)](\nabla h \cdot \nabla \Delta h), \end{aligned} \quad (4)$$

where  $d_h$  stands for derivatives with respect to  $h$  and  $\Delta, \Delta^2$  denote the horizontal Laplace and biharmonic operators, respectively. Here the “diffusion constant”  $D$  turns out to be

$$D(h) = Q(h)d_{hh}^2 f(h) \quad (5)$$

and a function of  $h$  itself. We note that using the  $h^4$  potential [10]  $f(h) = -h^2/2 + h^4/4$ , and a constant mobility  $Q = 1$ , Eq. (4) turns into the well-known Cahn-Hilliard equation [11]. Since  $\int d^2\mathbf{x} h = h_0$  is a conserved quantity under the evolution described by (1) or equivalently by (4), we may use  $h_0$  (the mean value of the height or the height of the flat film) as a control parameter in the following. From linear stability analysis it is clear that the homogeneous state  $h = h_0$  can get unstable via spatially periodic solutions if  $D(h_0) < 0$ . The lines  $D(h) = 0$  are named spinodals. Between the spinodals, instability sets in with the fastest growing wave vector  $|\mathbf{k}_c| = \sqrt{-D(h_0)/2Q(h_0)}$ . It is named type II<sub>s</sub> instability in the classification given by Cross and Hohenberg [12]. The same kind of linear instability is found in the Kuramoto-Sivashinsky equation [13].

*The disjoining pressure of Pismen and Pomeau.*—In a very recent work [4], the disjoining pressure

$$\Pi = -d_h f(h) = -\frac{2}{a} e^{-h/\ell} \left(1 - \frac{1}{a} e^{-h/\ell}\right) - \rho g h \quad (6)$$

was suggested. Here  $\rho$  is the density of the film and  $g$  the gravitational acceleration. In contrast to previous work, where the disjoining pressure is derived from intermolecular forces, only one free parameter,  $a$ , enters here ( $\ell$  can be scaled into  $h$ ). It describes the wetting properties of the film, for  $a > 0$  the density of the fluid decreases in a small boundary layer by approaching the solid surface. By derivation,  $a$  has to be a small quantity, and we fix it in the following at  $a = 0.1$ . Figure 1 shows the disjoining pressure for a certain  $g$ . The three heights that lay on

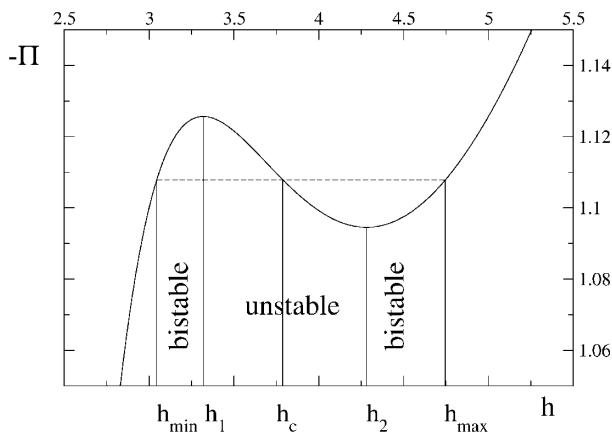


FIG. 1. The disjoining pressure of Pismen and Pomeau [4] for  $a = 0.1$ ,  $G = 0.2$ . The dashed line is obtained by an equal areas construction (cf. text).

the Maxwell line (dashed) may coexist, but the one in the middle is unstable to infinite disturbances. Below (above) a certain  $h_{\min}$  ( $h_{\max}$ ) (the binodals) only one height is possible and the flat film is absolutely stable. Between the two extrema  $h_1, h_2$  (the spinodals) the flat film is unstable to arbitrarily small disturbances. In regions between  $h_{\min}$  and  $h_1$  as well as  $h_2$  and  $h_{\max}$  the film is bistable, and drops or holes can be created only by a finite disturbance (nucleation regime) [14]. Therefore for certain mean heights, the film has two competing preferred thicknesses, one below and the other above the mean height, which can be realized locally. This can be understood in terms of the phase field theory. Assuming the fluid density  $\rho(z)$  as phase variable ( $\rho \approx 1$  means liquid,  $\rho \approx 0$  gas state), two steady stable kink solutions  $\rho_1(z), \rho_2(z)$  of the phase field equation (for details see [4])

$$\dot{\rho} = \partial_{zz}^2 \rho - \rho(1 - 2\rho)(1 - \rho) + a^2(\mu - Gz) \quad (7)$$

with the boundary condition  $\rho(0) = 1 - a$  at the solid support and  $\rho(\infty) = 0$  exist (Fig. 2), and  $G$  is the nondimensional gravitational constant. The kink marks the location of the (diffusive) interface. The two coexisting heights for a certain chemical potential  $\mu$  are found as  $h_{\min, \max} = \int_0^\infty \rho_{1,2} dz$ . After appropriate scaling to nondimensional variables, the mobility, derived from a Poiseuille flow, simply reads  $Q(h) = h^3$ . In this scaling expression (5) turns into

$$D(h) = h^3 \left( -\frac{2}{a} e^{-h} + \frac{4}{a^2} e^{-2h} + G \right). \quad (8)$$

Figure 3 shows the spinodals as well as the binodals for different  $G$ .

*Numerical solutions.*—Pattern formation on thin films was extensively studied in experiments over the last decades, for a review see [2] and [15,16]. To present numerical solutions, we solved (4) with (8) using a pseudospectral code which was developed earlier for the solution of 2D models describing convection patterns [17]. The code is implemented on an alpha workstation and allows for a spatial resolution up to  $256 \times 256$  mesh points. Because of the semi-implicit time integration, the time step could be fixed at values of order one. This allows computations for rather large domains in a reasonable time (some hours). Details of the numerical

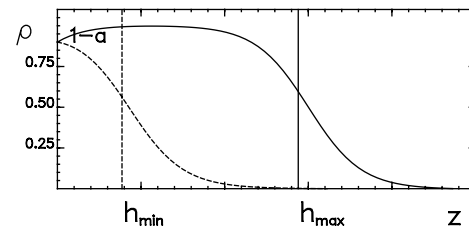


FIG. 2. Two numerically obtained coexisting kink solutions of the phase field equation (7), corresponding to two different film thicknesses with the same chemical potential.

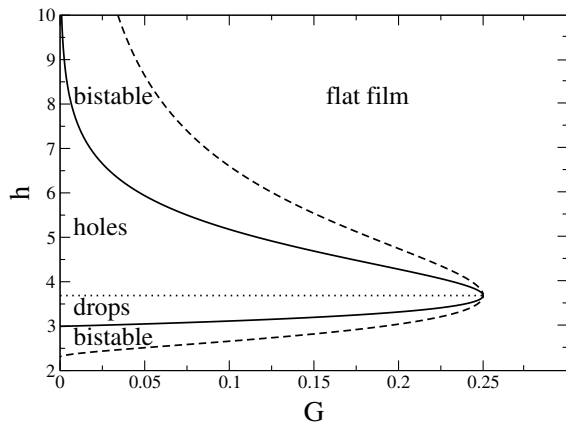


FIG. 3. Binodals (dashed) and spinodals (solid) as a function of  $G$ . The dotted line denotes  $h_c$ , the height which separates holes from drops (cf. text).

scheme will be presented elsewhere. For all runs we use fixed parameters  $G = 0.2$  and  $a = 0.1$ , and various values of the mean height  $h_0$ .

1. Spinodal decomposition, drops: Fig. 4, top row, shows a time series with  $h_0 = 3.4$  in the unstable region. On the time scale of the linear growth rate found from (4),  $\tau = 4Q(h_0)/D^2(h_0) \approx 200$ , small drops with wave vector modulus  $k_c \approx 0.1$  are formed, as expected for type II,

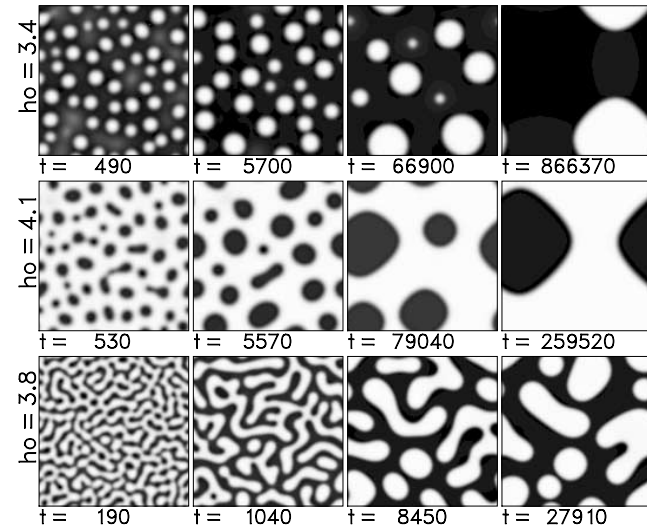


FIG. 4. Numerical results of (4) for different mean heights  $h_0$ . The film height is proportional to the brightness. Top row: formation of drops, side length of the layer  $L = 480$ ,  $128 \times 128$  mesh points. In the initial phase, small cells are formed. During the evolution, larger drops grow at the expense of the smaller ones which vanish. Drops are usually always circular. The squarelike shape in the last frame is probably due to self-interaction, which is possible for periodic lateral boundary conditions. Middle row: formation of holes. The same dynamics as for drops can be seen in earlier stages. However, holes are not always circular but like to form long and narrow structures.  $L = 480$ ,  $128 \times 128$  points. Bottom row: Mazes are formed in an earlier stage for intermediate values of  $h_0$  near  $h_c$ . Finally, drops survive.  $L = 650$ ,  $256 \times 256$  points.

instability. In the long time limit, smaller drops vanish or fuse to bigger ones, as a consequence of minimization of (3). If one waits long enough and the drops are not separated too much in space, only one big drop will eventually survive. The amplitude of the drops is roughly that of the upper binodal, where the height of the rest of the film coincides with the lower ones.

2. Spinodal decomposition, holes: The situation is opposite for larger  $h_0 = 4.1$  (Fig. 4, middle row). At the beginning, holes are formed with about the same  $k_c$  and on about the same time scale. In the long time limit one big hole will survive. During the evolution, the form of the holes is often not completely circular like that of drops. Instead the tendency to long, narrow holes can be clearly seen.

3. Spinodal decomposition, labyrinths: A mazelike structure in the short time range is formed for intermediate  $h_0 = 3.8$  (Fig. 4, bottom row), giving way to drops for longer times.

The critical height  $h_c$  where drops change to holes in the long time limit can be found by the Maxwell construction done in Fig. 1. It coincides with the location of the local maximum of the free energy separating the two minima and corresponds to the middle intersection of the Maxwell line with the disjoining pressure. Its value depends on  $G$  and is plotted in Fig. 3 as a dotted line.

4. The falling film, separation of drops. Next we incline the film layer in the  $y$  direction by a small angle  $\alpha$ , giving

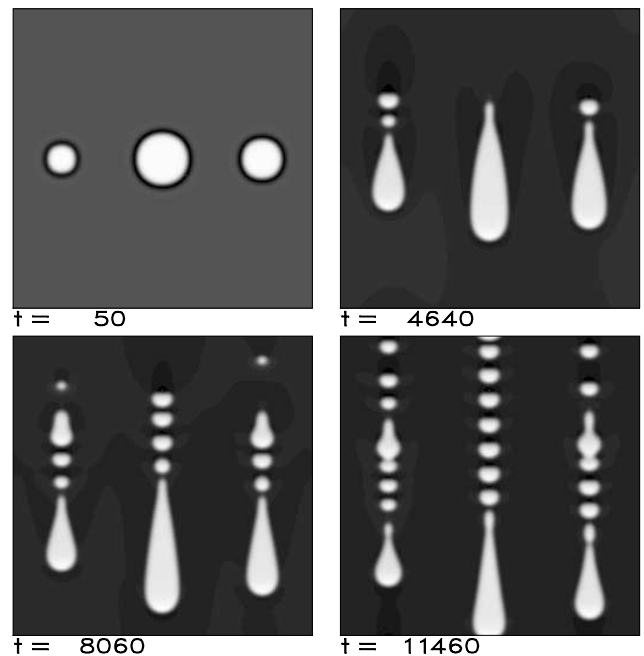


FIG. 5. The layer is now inclined in the  $y$  direction, and the film falls downwards. Larger drops travel faster. For large enough inclination angle, secondary drops separate from the primary ones. We fixed  $h_0 = 3.2$  in the bistable region to avoid instability of the flat domains.  $L = 950$ ,  $256 \times 256$  points.

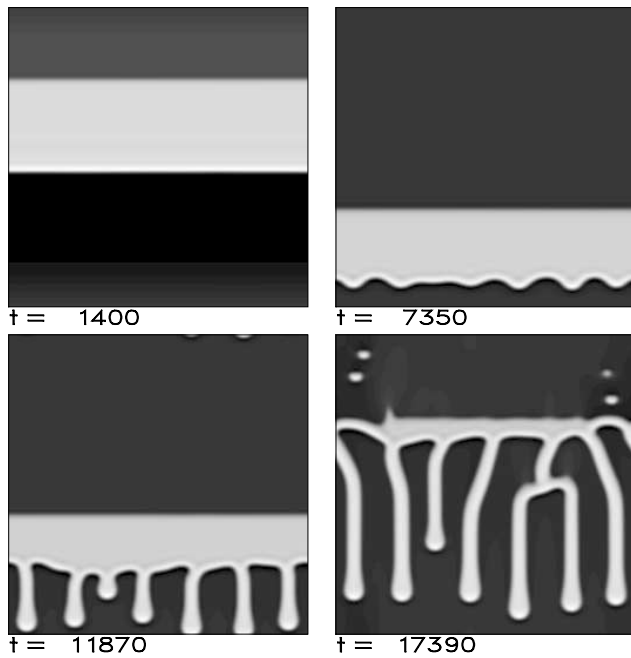


FIG. 6. Falling film, where the initial condition is a wall. The leading front becomes unstable by a periodic instability and fingering can be observed.  $L = 950$ ,  $256 \times 256$  points.

an additional force term [2]. In nondimensional form, the current (2) has to be extended:

$$S(h) = -Q(h)[\nabla\phi(h) + \alpha G\mathbf{e}_y], \quad (9)$$

where  $\mathbf{e}_y$  is the unit vector in the  $y$  direction. Starting the simulation with only a few drops, cusps are formed at their trailing ends for not too large  $\alpha$ . For larger values, the cusps get sharper and small drops separate (Fig. 5). The velocity increases with the size of the drops. On smaller drops the cusps are generated faster and the separation of secondary drops is seen earlier.

5. The falling film, fronts, and fingers: Finally, we study the instability of a falling front. Let  $L$  be the length of the layer [in adimensional units of (8)]. As initial condition we take a wall of area size  $d \times L$ , homogeneous in the  $x$  direction. The height of the wall is that of the upper binodal  $h_{\max}$ , whereas the rest of the film has the height  $h_{\min}$ . The length  $d$  is chosen so that the mean height  $h_0 = (d/L)h_{\max} + (1 - d/L)h_{\min} = 3.4$ , in the unstable region. For  $\alpha = 0.2$  the leading front of the wall gets unstable by a periodic instability along the wall (Fig. 6). From this perturbation, fingers grow having more or less equal distances. The wave vector for the fingers for our parameters is  $k \approx 0.05$  which is about half of the critical wave vector. We note that we also observed an unstable trailing edge of the wall, but for smaller values of  $\alpha = 0.1$ .

Qualitatively the same pictures are obtained in experiments with falling films of silicone oil or glycerine [9,18], and numerically in a very recent work with a different disjoining pressure [19].

In conclusion, we found that our numerical simulations using the disjoining pressure of [4] can explain the formation of three dimensional drops and holes near a three phase contact line. We determined the critical height, below (above) which the flat film is unstable and forms drops (holes). Finally, for inclined films we predict the deformation of circular drops followed by separation of secondary smaller drops at the trailing end as well as finger formation along initially straight fronts.

We acknowledge helpful discussions with Dr. U. Thiele. The work was partially supported by the EU through TMR Grant No. FMRX-CT96-0010.

\*Email address: bes@physik.tu-cottbus.de

- [1] A. Vrij, *Discuss. Faraday Soc.* **42**, 23 (1966).
- [2] A. Oron, S. H. Davis, and S. G. Bankoff, *Rev. Mod. Phys.* **69**, 931 (1997).
- [3] D. M. Anderson, G. B. McFadden, and A. A. Wheeler, *Annu. Rev. Fluid Mech.* **30**, 139 (1998).
- [4] L. M. Pismen and Y. Pomeau, *Phys. Rev. E* **62**, 2480 (2000).
- [5] To be more exact, type IV systems have no long range attraction, which coincides with the disjoining pressure used here for the case of vanishing gravitation.
- [6] A. Sharma and R. Khanna, *Phys. Rev. Lett.* **81**, 3463 (1998).
- [7] A. Sharma and R. Khanna, *J. Chem. Phys.* **110**, 4929 (1999).
- [8] G. Reiter, A. Sharma, A. Casoli, M.-O. David, R. Khanna, and P. Auroy, *Langmuir* **15**, 2551 (1999).
- [9] M. F. G. Johnson, R. A. Schluter, M. J. Miksis, and S. G. Bankoff, *J. Fluid Mech.* **394**, 339 (1999).
- [10] A. Novick-Cohen and L. A. Segel, *Physica (Amsterdam)* **10D**, 277 (1984).
- [11] J. W. Cahn and J. E. Hilliard, *J. Chem. Phys.* **28**, 258 (1958).
- [12] M. C. Cross and P. C. Hohenberg, *Rev. Mod. Phys.* **65**, 581 (1993).
- [13] Y. Kuramoto and T. Tsuzuki, *Prog. Theor. Phys.* **55**, 356 (1976); G. I. Sivashinsky, *Acta Astronaut.* **4**, 1177 (1977).
- [14] U. Thiele, K. Neuffer, Y. Pomeau, and M. G. Velarde (to be published).
- [15] G. Reiter, *Phys. Rev. Lett.* **68**, 75 (1992).
- [16] G. Reiter, *Langmuir* **9**, 1344 (1993).
- [17] M. Bestehorn, *Phys. Rev. E* **48**, 3622 (1993).
- [18] H. E. Huppert, *Nature (London)* **300**, 427 (1982).
- [19] J. A. Diez and L. Kondic, *Phys. Rev. Lett.* **86**, 632 (2001).